Journal of Nanobiotechnology

RESEARCH

Open Access

Dual-responsive renal injury cells targeting nanoparticles for vitamin E delivery to treat ischemia reperfusion-induced acute kidney injury

Jiahao Zhang[1,2†], Xi Ren[3,4†], Zhaoyang Nie[4†], Yue You[1,2], Yao Zhu[1], Hui Chen[1], Haichuan Yu[1], Gaozhi P. Mo[1], Lianjiu Su[1,2,5*], Zhiyong Peng[1,2,6*] and Man-Chung Tang[4*]

Abstract

Ischemia/reperfusion (I/R) is an important inducer of acute kidney injury (AKI), and triggers the generation of reactive oxygen species (ROS) and the expression of matrix metalloproteinase 2 (MMP2), exacerbating kidney damage. Given the immense potential of vitamin E (VitE) as a natural fat-soluble antioxidant in kidney protection, we designed the nanoparticles (NPs) that could dual respond to ROS and MMP2, aiming to accurately deliver VitE to renal injury cells. The NPs utilized Gel-SH as a sensitive receptor for MMP2 and diselenide as a sensitive receptor for ROS, while PEG_{2k} modification enhanced biocompatibility and prevented phagocytosis mediated by the mononuclear phagocyte system. The amphiphilic Gel-SH and diselenide encapsulate the liposoluble VitE and self-assemble into the NPs with a hydrodynamic size of 69.92 nm. Both in vivo and in vitro experiments based on these NPs show good biocompatibility and the ability of target renal injury cells. In vivo kidney I/R injury models and in vitro cell hypoxia/reoxygenation models, the NPs have demonstrated effects in reducing oxidative stress and alleviating AKI. Notably, VitE can preferentially react with peroxyl radical (LOO•) than polyunsaturated fatty acid (PUFA), inhibiting the formation of carbon centered radical (L•), thereby blocking the chain reaction between PUFA and LOO• in ferroptosis. The NPs also inhibit the transition from AKI to chronic kidney disease, with few side effects. Thus, the NPs with dual-responsiveness to MMP2 and ROS for targeted delivery of VitE to renal injury cells exhibit remarkable effects in inhibiting ROS and the chain reactions of ferroptosis, making it a promising therapeutic agent against AKI caused by I/R.

Keywords Acute kidney injury, Ischemia/reperfusion, Nanoparticle, Vitamin E, Ferroptosis

†Jiahao Zhang, Xi Ren and Zhaoyang Nie have contributed equally to this study and therefore shared the first author role.

*Correspondence:
Lianjiu Su
sulianjiu@whu.edu.cn
Zhiyong Peng
pengzy5@hotmail.com
Man-Chung Tang
kobetang2021@sz.tsinghua.edu.cn
Full list of author information is available at the end of the article

Graphical abstract

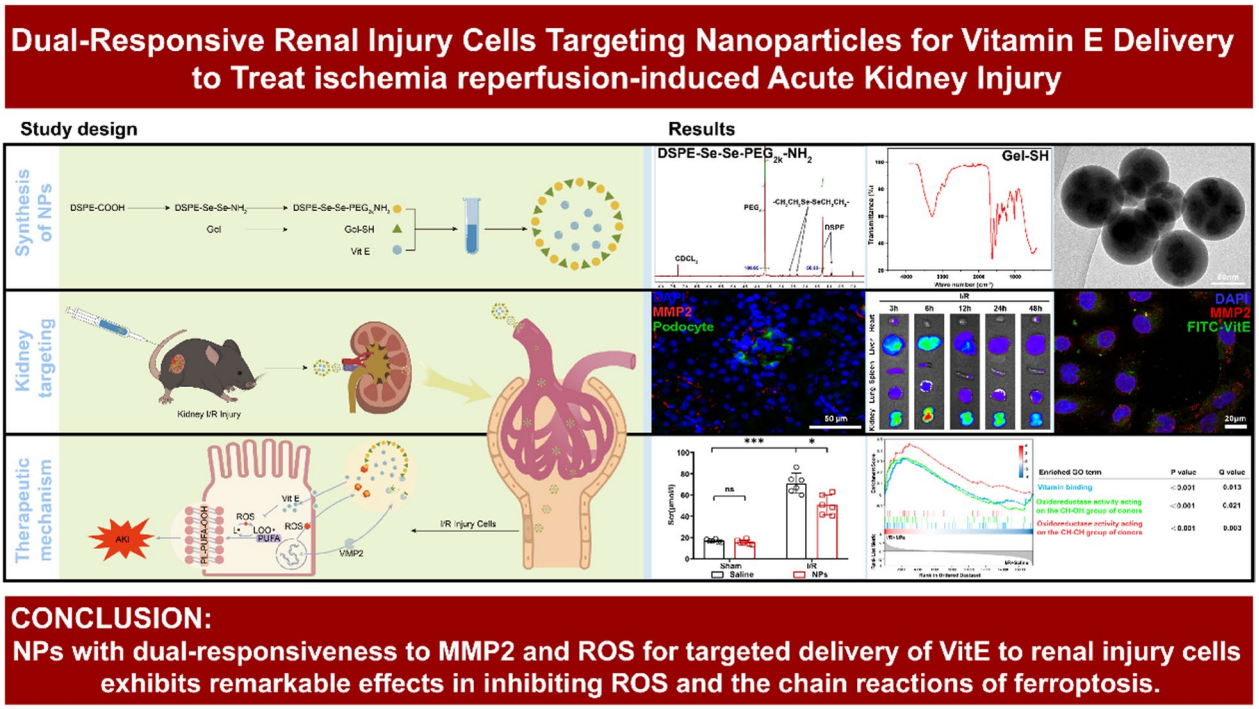

Introduction

Acute kidney injury (AKI) is a series of pathological and physiological changes caused by sudden decline in renal function and inability to eliminate metabolic waste in the body, usually caused by renal ischemia/reperfusion (I/R), sepsis, and nephrotoxin [1–3]. AKI occurs in about 13.3 million people per year, thereby contributing to about 1.7 million deaths every year [4]. However, there is a significant lack of specific and effective treatment for AKI, among surviving AKI patients, nearly 70% of them will progress to chronic kidney disease (CKD) and renal failure, requiring lifelong dialysis [5]. Therefore, it is highly desirable to explore effective therapies for AKI.

Lipid peroxidation is the oxidation of phospholipids with polyunsaturated fatty acid (PUFA) tails in an iron dependent manner. A peroxyl radical (LOO•) abstracts a hydrogen (H) from PUFA and forms a lipid hydroperoxide (LOOH), but also generates carbon centered radical (L•), which will react with oxygen to form another LOO• and form a chain reaction [6, 7]. The mitochondrial density and oxygen consumption of the kidneys are second only to those of the heart [8, 9]. Oxidative stress-induced ferroptosis plays a crucial role in I/R-AKI [10, 11]. Inhibiting oxidative stress-induced ferroptosis is a potential target for AKI treatment.

Vitamin E (VitE) is the main lipophilic antioxidant in the body. VitE could attenuate ferroptosis via the termination of chain reaction by inhibiting L• formation [12, 13]. Despite VitE's immense therapeutic promise in kidney diseases, its clinical application remains constrained due to its limited bioavailability and high concentrations required for administration, which can subsequently elevate patient mortality [13, 14]. Relevant studies have shown that nanoparticles (NPs) with kidney targeting capabilities can enhance bioavailability and local drug concentration in the kidney, while minimizing toxic side effects [1, 15, 16]. Targeted supplementation of VitE represents an effective strategy for the treatment of AKI.

In our study, we designed a renal targeting system by employing diselenide and Gel-SH as shells, encapsulating VitE to create 69.92 nm NPs. The mesangial space can be directly accessed through the glomerular vascular fenestrations, which typically exhibit a relatively wide width of 70 to 130 nm [17]. Previous studies have demonstrated significant changes in the structure and permeability of the glomerular filtration barrier (GFB) in I/R, thereby allowing the passage of smaller than 100 nm [18]. Metalloproteinases (MMPs), particularly MMP2, are overexpressed and released in renal injury cells, participating in the degradation of extracellular

matrix and exacerbating AKI. Gel, as a substrate of MMP2, can be degraded by renal injury cells that secrete MMP2. Selenium is an important component of the antioxidant glutathione peroxidase in the body. The diselenide could be cleaved by oxidants and is an important candidate for oxidation reactions. We employed Gel-SH and diselenide for the dual-responsive release of VitE to MMP2 and ROS, achieving targeted VitE delivery to renal injury cells. The NPs have been evaluated both in vitro and in vivo and showed significant effects on AKI. Specifically, VitE can preferentially react with LOO• than PUFA, inhibiting the formation of L•, thereby blocking the chain reaction between PUFA and LOO• in ferroptosis (Fig. 1).

The amphiphilic Gel-SH and DSPE-Se-Se-PEG_{2k}-NH_2 encapsulate the liposoluble VitE and self-assemble into the NPs with a hydrodynamic size of 69.92 nm. After tail vein injection, NPs could effectively accumulate in kidney and pass through glomerular filtration barrier disrupted by I/R. The NPs with dual-responsive to MMP2 and ROS are designed for targeted delivery of VitE to renal injury cells. The targeted delivery of VitE could block the chain reaction between PUFA and LOO• in ferroptosis and alleviate AKI.

Methods

Materials

The materials are described in Supplementary Table 1. Antibodies for western blotting are described in Supplementary Table 2. Primer sequences for RT-PCR are described in Supplementary Table 3.

Synthesis of DSPE-Se-Se-PEG_{2k}-NH_2

Synthesis of DSPE-COOH

DSPE (100 mg) and succinic anhydride (14.7 mg) were dissolved in triethanolamine solution and reacted at room temperature for 10 min. The product mixture was concentrated by rotary evaporation and the crude product was precipitated by cold acetone. The above steps were repeated twice to improve the purity of the crude product. And then the crude product was subjected to column chromatography to isolate pure DSPE-COOH.

Synthesis of DSPE-Se-Se-NH-Boc

DSPE-COOH (100 mg), EDC (38 mg), and DMAP (24 mg) were dissolved in anhydrous DMSO (20 mL) with a molar ratio of 1:1.5:1.5. The mixture was stirred for 30 min in an argon atmosphere at 0 °C to activate the carboxyl groups of DSPE-COOH. Meanwhile, n-Boc-NH-CH_2CH_2-Se-Se-CH_2CH_2-NH_2 (45 mg) was dissolved in

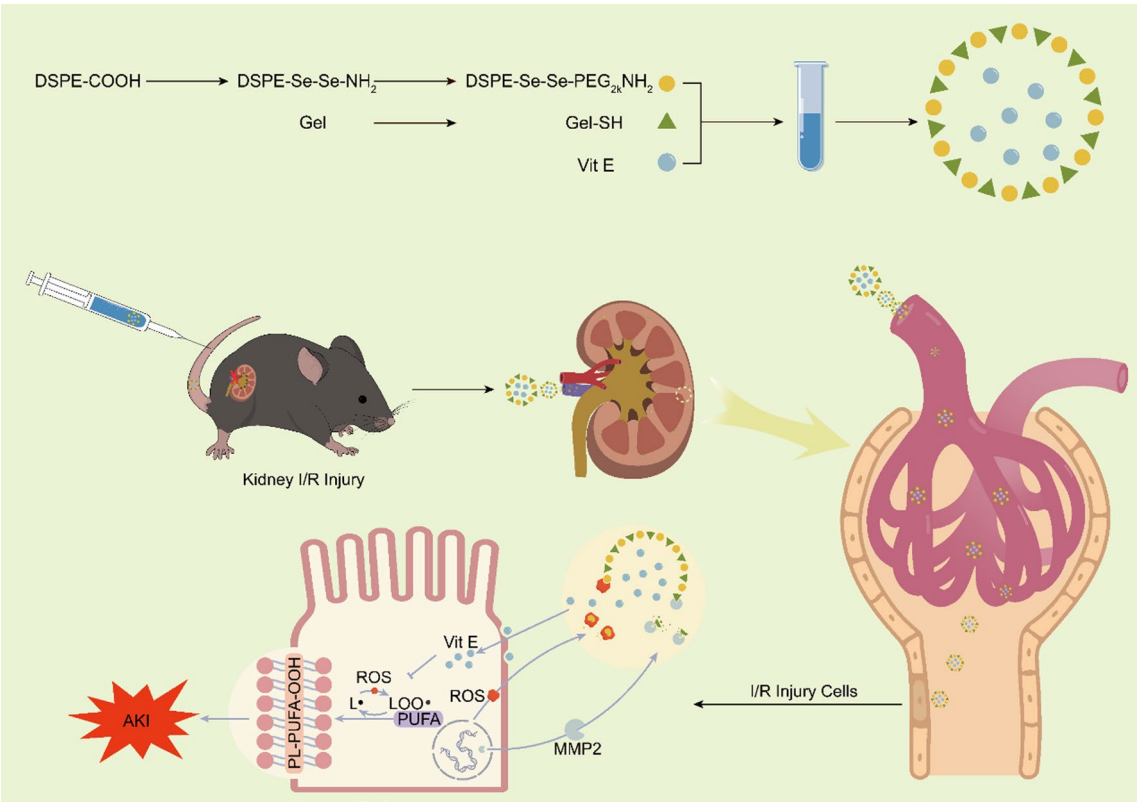

Fig. 1 The structure of NPs and the schematic illustration for NPs to reduce ferroptosis and alleviate I/R-AKI

DMSO at a molar ratio of 1:1 with DSPE-COOH. Then n-Boc-NH-CH_2CH_2-Se-Se-CH_2CH_2-NH_2/DMSO solution was slowly injected into the activated DSPE-COOH solution, react at room temperature in the dark for 48 h. After the reaction, the product was purified by dialysis (MWCO 1000 Da) to obtain DSPE-Se-Se-NH-Boc.

Synthesis of DSPE-Se-Se-NH_2

DSPE-Se-Se-NH-Boc (100 mg) was dissolved in TFA (10 mL) and stirred at room temperature for 30 min to remove the Boc. The mixture was then concentrated using rotary evaporation, and the product was purified by dialysis (MWCO 1000 Da) to obtain pure DSPE-Se-Se-NH_2.

Synthesis of DSPE-Se-Se-PEG_{2k}-NH-Boc

DSPE-Se-Se-NH_2 (100 mg) and Boc-NH-PEG_{2k}-NHS (242 mg) were dissolved in TFA (30 mL with a molar ratio of 1:1, and were allowed to react at room temperature for 10 min. After the reaction, the mixture was then concentrated using rotary evaporation, and the product was purified by dialysis (MWCO 2000 Da) to obtain pure DSPE-Se-Se-PEG_{2k}-NH-Boc.

Synthesis of DSPE-Se-Se-PEG_{2k}-NH_2

DSPE-Se-Se-PEG_{2k}-NH-Boc (100 mg) was dissolved in TFA (10 ml), and stirred at room temperature for 45 min to remove Boc. After reaction, After the reaction, the mixture was then concentrated using rotary evaporation, and the product was purified by dialysis (MWCO 2000 Da) to obtain pureDSPE-Se-Se-PEG_{2k}-NH_2.

Synthesis of Gel-SH

Gelatin was synthesized according to the reported method [19]. Under ultrasonic conditions, the gelatin aqueous solution (10 mg/ml) was added to the activation solution with deionized water (800 μl), hydroxide solution (800 μl, 0.1 M), and anhydrous ethanol (400 μl) containing mercaptobenzoic acid (0.008 g, 0.05 mmol) and EDC (0.010 g, 0.05 mmol). The mixture was reacted at 40 °C for 4 h under a N_2 atmosphere. After the reaction, the mixed solution was first purified by dialysis against DMSO and then against deionized water for 24 h (MWCO = 8000–14000) to obtain Gel-SH. Fixed-SH content was calculated via absorbance. Gel-SH (0.020 g) was dissolved in pH 8.0 Tris–glycine buffer (8 ml), and then 0.1 mL of sodium dodecyl sulfate (0.5%, SDS) and 0.02 mL of Ellman's reagent were added. The resulted mixture was diluted to 10 ml and incubated in a water bath at 37 °C for 3 h. The absorbance was measured at a UV absorption with wavelength of 412 nm.

Characterization of NPs

The ^{1}H-NMR ($CDCl_3$) was confirmed by AVANCE NEO 400 M (Bruker, Germany), the FT-IR by Nicolete iS50 (Thermo, USA), transmission electron microscopy (TEM) by JEM F200 (JEOL, Japan), and the hydrodynamic size and zeta potentials by 90plus PALS (Nano-Brook, USA).

Drug loading content were analyzed by a fluoromax spectrometer with the excitation wavelength set at 530 nm and then calculated following Drug loading = (mass of VitE/mass of NPs) × 100%.

To investigate the release profile of encapsulated VitE in vitro, 10 mL of NPs micelles solution was sealed into a dialysis bag (MWCO 3500 Da), then immerged in 100 mL of phosphate buffered solution (PBS, pH 7.4) with or without H_2O_2 and MMP2, and incubated at 37 °C with a constant stirring. Collect one milliliter dialysate at different time intervals while complement the same volume of fresh medium back to keep dialysis volume unchanged. The concentration of the released VitE was measured through fluoromax spectrometry.

Cell culture and hypoxia/reoxygenation model

HK-2 cells were from the Cell Bank of the Chinese Academy of Sciences. Cultured in MEM (HyClone) with 5 ng/ml human recombinant EGF (Novus), 10% FBS (Gibco) and penicillin–streptomycin supplement.

For hypoxia/reoxygenation (H/R) model, after medium was changed to serum and glucose-free MEM, cellular hypoxic conditions were created in a modular incubator chamber (Biospherix, Lacona, NY, USA) with 1% O_2, 5% CO_2 and 94% N_2. Cells were incubated under normal conditions for 60 min after the indicated times of H/R.

Animals, kidney I/R model and in vivo distribution of NPs

Institute of C57BL/6 mice were provided from Center for Animal Experiment of Wuhan University and randomly divided into four groups (6 mice/group). Mice 8–10 weeks old males, raised under specific pathogen-free and controlled temperature with 12 h light/dark cycle. All animal experiments were approved by The Animal Care and Use Committee of Zhongnan Hospital of Wuhan University and the approved number was WP20230685. Additionally, all animals were provided humane treatment according to the ARRIVE guidelines [20].

For kidney I/R surgery, mice were anesthetized with isoflurane, abdomen opened after iodine disinfection, bilateral renal pedicles occluded with microvascular clamp, clamp removed after 30 min ischemia for reperfusion. If the clamp became dislodged prematurely, or if the animal died prematurely, preventing the collection

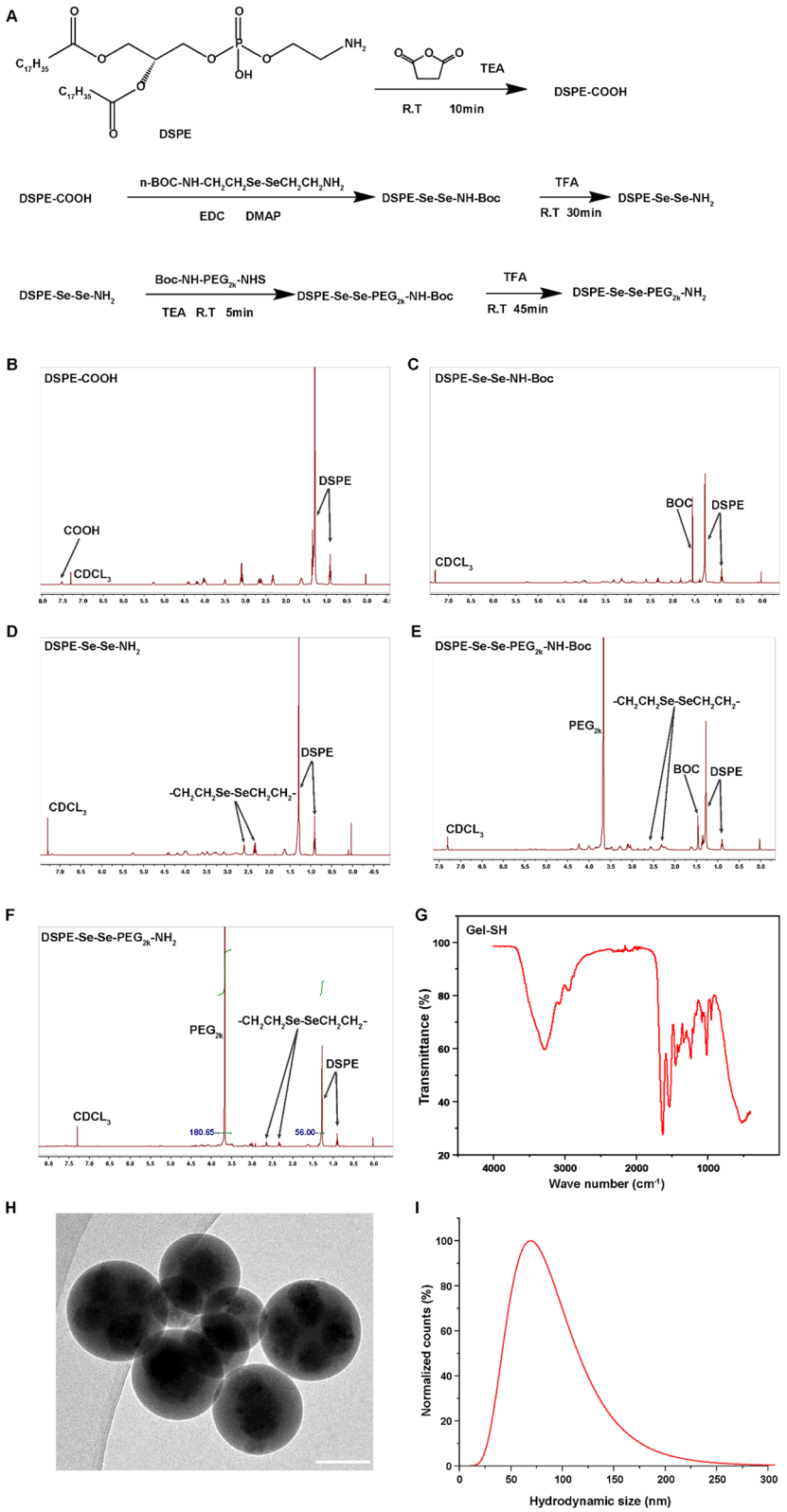

Fig. 2 Syntheses and Characterization of NPs. **A**. Syntheses methods of DSPE-Se-Se-PEG_{2k}-NH_2. **B**. ^{1}H-NMR ($CDCl_3$) spectrum of DSPE-COOH. **C**. ^{1}H-NMR ($CDCl_3$) spectrum of DSPE-Se-Se-NH-Boc. **D**. ^{1}H-NMR ($CDCl_3$) spectrum of DSPE-Se-Se-NH_2. **E**.^{1}H-NMR ($CDCl_3$) spectrum of DSPE-Se-Se-PEG_{2k}-NH-Boc. **F**. ^{1}H-NMR ($CDCl_3$) spectrum of DSPE-Se-Se-PEG_{2k}-NH_2. **G**. FT-IR spectrum of Gel-SH. **H**. Representative TEM images of NPs, scale bar = 50 nm. I. Hydrodynamic size of NPs.

of behavioral and histological data. In Sham group, mice were subjected to same process without clamping. To aid in recovery, prewarmed saline (0.05–0.1 mL/g body weight) was injected subcutaneously. After the procedure, the animals were placed on a warming blanket and given postoperative analgesia once they had fully recovered from anesthesia.

For in vivo distribution of NPs, mice were euthanized at different time after sham or surgery to collect major organs. The organs were visualized and the relative fluorescence value was calculated by the IVIS Lumina LT Series III (PerkinElmer, America).

Cell viability assay

HK-2 cells were plated in 96-well plates, and treated with NPs at different concentrations for different times. Cell viability was evaluated by Cell Counting Kit 8 (Dojindo Molecular Technologies, Kumamoto, Japan).

Blood detection

Heparinized blood was centrifuged at 2000 rpm for 10 min to obtain plasma. The plasma was tested by hematology analyzer (BC-5000vet, Mindray, Shenzhen, China) and automatic biochemical analyzer (Chemray 800, Rayto, Shenzhen, China).

Immunohistochemical and immunofluorescence staining

Paraffin-embedded kidney Sects. (4 μm) were deparaffinized, antigen retrieval with ethylene diamine tetra acetic acid (1 mM), H_2O_2 (0.03%) for immunohistochemical study, primary antibody incubated overnight at 4 °C. For immunofluorescence, slides with primary antibodies at

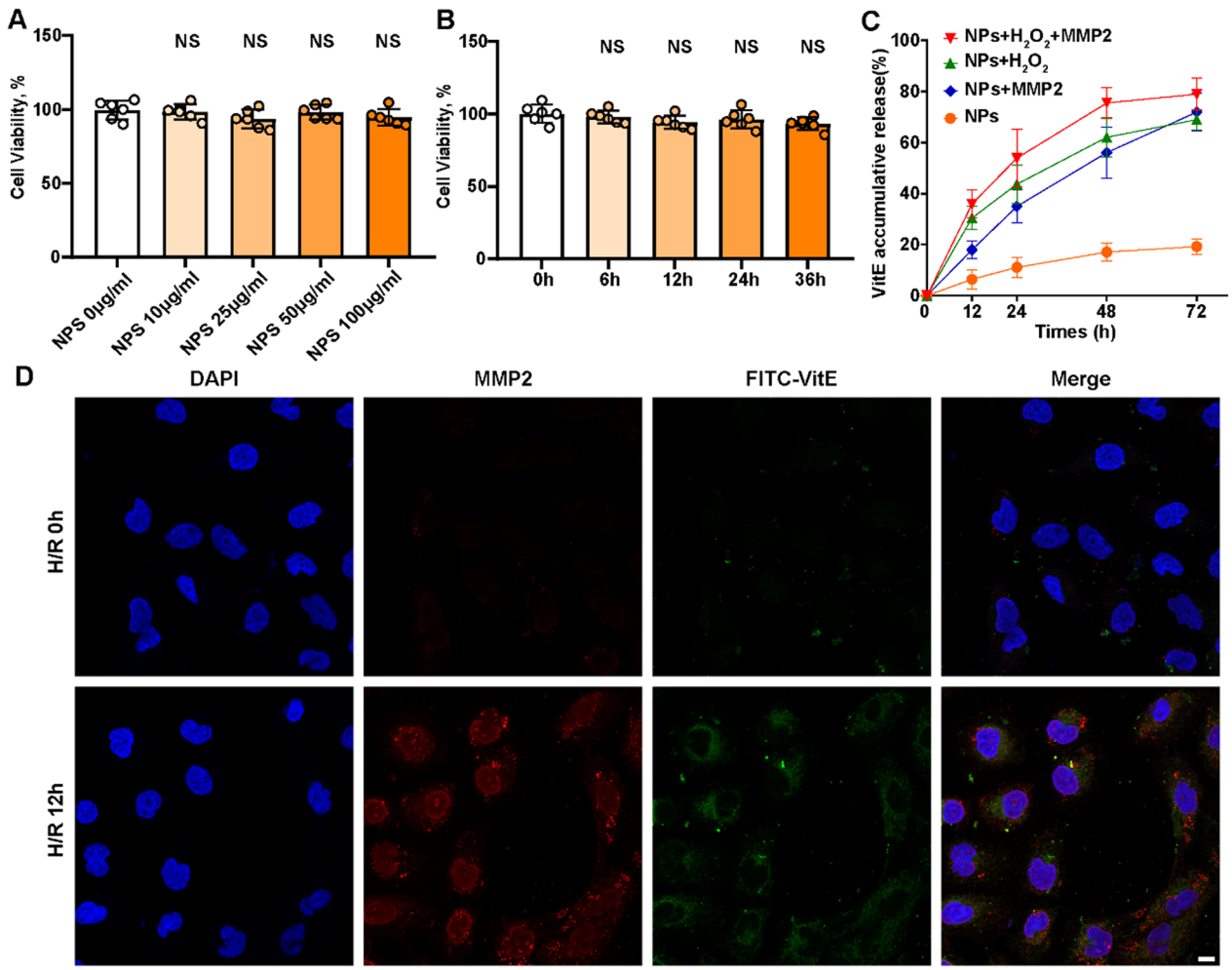

Fig. 3 Biocompatibility, Cellular Uptake, and Targeted Ability of NPs Fig. 3. Biocompatibility, Cellular Uptake, and Targeted Ability of NPs. **A**. The dose-dependent cytotoxicity tests of NPs on HK-2 cells in vitro. **B**. The time-dependent cytotoxicity tests of NPs on HK-2 cells in vitro. **C**. The in vitro drug release curves of the NPs. **D**. Representative confocal microscopy images of MMP2 and FITC-VitE in HK-2 cells, scale bar = 10 μm. Results are presented as means ± SEM, n = 6. P values from One-way ANOVA with Dunnett's multiple comparisons test

4 °C overnight, images detected by fluorescence microscopy, positive images analyzed by digital image analysis using Image J.

HK-2 cells cultivated on slides for staining, slides with primary antibodies at 4 °C overnight, after secondary antibody, images detected by confocal or fluorescence microscopy.

Histopathology and TUNEL detection

Tissue was fixed with 4% PFA, and sectioned for Haematoxylin and eosin (HE) staining. The Apoptosis Detection Kit (S7100, Serologicals, Millipore) was used to detect TUNEL positive cells.

DHE staining

After harvested, kidney tissue was placed in frozen section embedding agent (Yeasen) and rapidly frozen in liquid nitrogen. Frozen tissue sections were incubated at 37 ℃ with 10 μM DHE for 30 min, and analyzed by fluorescence microscopy.

Western blotting and quantitative RT-PCR

Western blotting was used to measure protein expression in tissues and cells. Image J was used to quantify the protein expression. In addition, mRNA RT was performed with ReverTra Ace kit (Toyobo, Osaka, Japan). All reactions were run in RT-PCR Detection System (Bio-Rad).

RNA sequencing analysis

Total RNA was extracted from kidney of mice. The RNA library was sequenced on the BGISEQ-500 platform (BGI Genomics, Shenzhen, China). Differentially expressed genes (DEGs) were screened using two criteria: (1) a fold change greater than 1.5 and (2) a corresponding adjusted P value < 0.05. KEGG analysis with a P value < 0.05 were considered significantly enriched. The analysis of DEGs and KEGG pathways was performed at Dr.tom online (https://biosys.bgi.com).

Flow cytometry

After treatment, 10^6 cells were collected, centrifuged and discarded the supernatant. ROS was detected by ROS kit (40778ES50, Yeasen). Fluorescence was analyzed using a flow cytometer.

Statistical analysis

All numerical data was expressed as means ± SEM. Student's t test and One-way ANOVA were used. Statistical analyses were performed using SPSS (version 22.0), and GraphPad Prism (version 8.0). P value < 0.05 was considered to be statistically significant.

Results

Syntheses and characterization of NPs

As shown in Fig. 2A, we employed diselenide as the reaction site for drug release, modified PEG_{2k} to avoid mononuclear phagocyte system mediated phagocytosis, and synthesized DSPE-Se-Se-PEG_{2k}-NH_2, in steps. Meanwhile, the introduction of the diselenide bond enhances the oil solubility of the polymer, while the PEG fragment improves the water solubility. The ^{1}H-NMR spectra of the intermediates and the target compounds have been shown in Fig. 2B–F. In addition, based on reported study, we modified hydrophilic Gel to amphiphilic Gel-SH by grafting hydrophobic 4-mercaptobenzoic acid onto the gelatin molecules through an amide bond. The red-shift observed in the FT-IR spectrum at 1650 cm^{-1} was attributed to the association of Gel-SH through π-π stacking interactions between the benzene rings of 4-mercaptobenzoic acid. This verified the successful grafting of 4-mercaptobenzoic acid onto Gel molecules (Fig. 2G) [19]. The content of thiol in Gel-SH was determined by Ellman method and was 60.13 μmol/g (Fig. S1A). Finally, Gel-SH, DSPE-Se-Se-PEG_{2k}-NH_2, and VitE were self-assembled in the saline or PBS. TEM proved that it could stably assemble into spheres and encapsulate VitE, and the drug loading was 19.1% ± 5.9% (Fig. 2H). Dynamic light scattering (DLS) illustrated that the hydrodynamic size of the resulting micelles was 69.92 nm (Fig. 2I). Zeta-potential results showed that the NPs had weak positive potential charge of being + (8.1 ± 2.4) mV (Fig. S1B). The weak positive charge facilitated the binding of nanoparticles to the cell surface, meanwhile with little cytotoxicity [16].

Biocompatibility, release, and cellular uptake of NPs in vitro

We performed a dose- and time-dependent cytotoxicity validation on HK-2 cells by CCK8. NPs didn't show cytotoxicity after 12 h of cultivation with a gradient

(See figure on next page.)

Fig. 4 Biocompatibility, Cellular Uptake, and Targeted Ability of NPs. **A**. Representative fluorescence microscopy images of MMP2 and Podocyte in kidney, scale bar = 50 μm. **B**. Representative fluorescence images of the main organs (heart, liver, spleen, lung and kidney) of Sham and I/R groups at 3, 6, 12, 24 and 48 h after tail vein injection of NPs-CY5.5. **C**. Average radiance of the main organs in Sham group. **D.** Average radiance of the main organs in I/R group. **E**. Representative fluorescence images for FITC-NPs of the main organs (heart, liver, spleen, lung and kidney) of Sham and I/R groups, scale bar = 20 μm. Results are presented as means ± SEM, n = 6

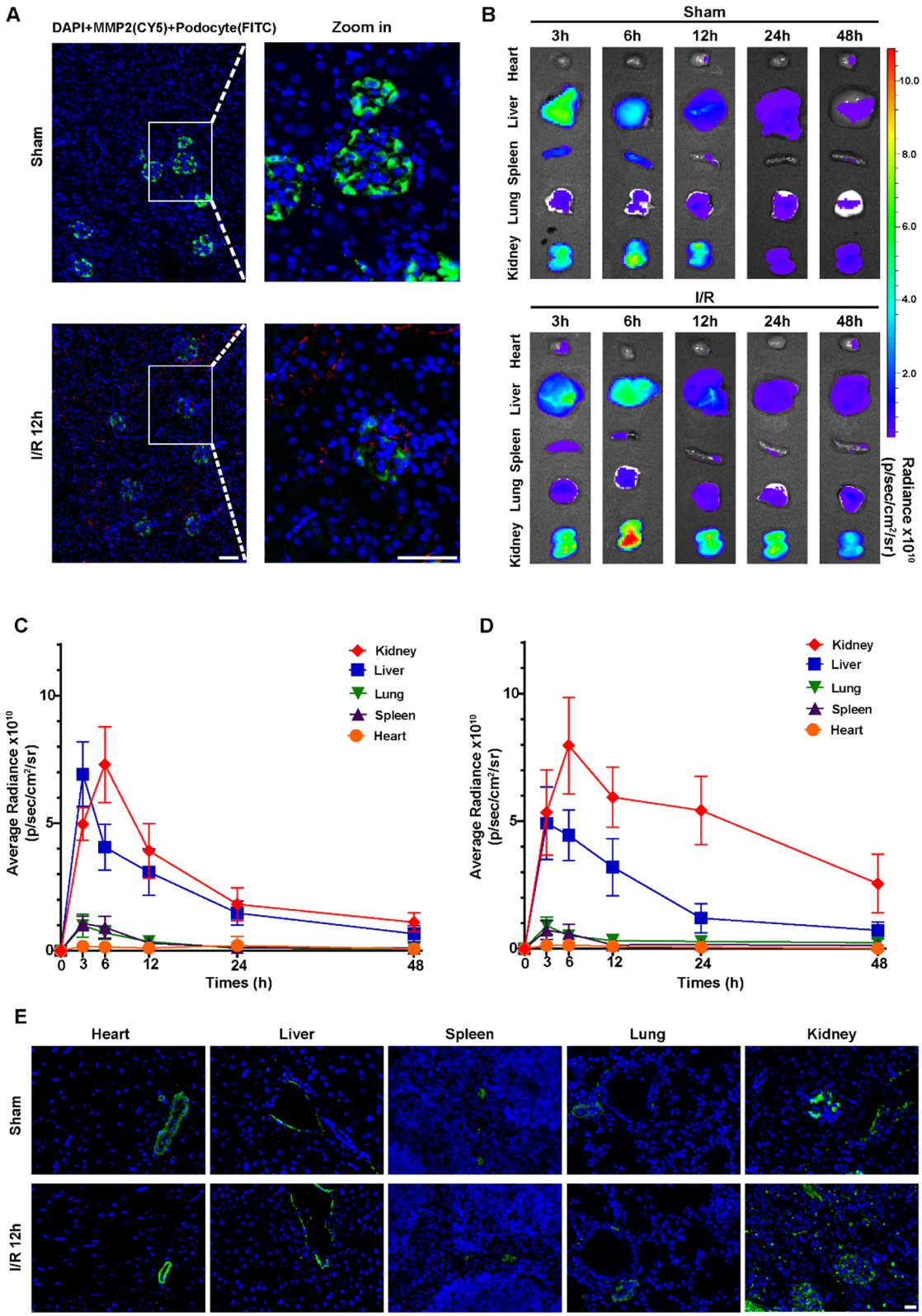

Fig. 4 (See legend on previous page.)

concentration and exposure to 50ug/ml (Fig. 3A, B). To investigate the dual-responsive release behavior of NPs, the in vitro VitE release curves with or without MMP2 and H_2O_2 were studied using a dialysis bag. The NPs could stably exist in the solution, and after 72 h, only about 19.26% of VitE was released from NPs, indicating that NPs could be stable during circulation. However, in the oxidative environment and under the action of MMP2, the release rates of NPs at 24 h, 48 h, and 72 h were 53.92%, 75.56% and 78.98%, respectively (Fig. 3C). The in vitro release results demonstrated that NPs with dual-responsiveness to MMP2 and ROS for targeted delivery of VitE to renal injury cells. To evaluate the cellular uptake ability of NPs, we used FITC-VitE encapsulated in NPs shell, and performed MMP2 fluorescence staining on HK-2 cells after 12 h of H/R. The laser confocal microscopy results showed that cells expressed MMP2 after H/R, and the cells absorbed VitE released from NPs' shell degraded by ROS and MMP2 (Fig. 3D).

Biocompatibility and targeted ability of NPs in vivo

C57 mice were used for in vivo biocompatibility testing. After 24 h of tail vein injection of 200ul (2 mg/kg), there was no damage to the tissue (Fig. S2A). Blood tests also showed no significant abnormalities (Fig. S2B). The expression of MMP2 in mouse glomeruli and changes in GFB (Nephrin) were detected by immunofluorescence. In Sham group, the GFB had an intact structure and almost no MMP2 expression was detected. After I/R, MMP2 was expressed, and GFB was disrupted, which allowed the passage and accumulation of NPs (Fig. 4A). At the same time, we used the shell wrapped CY5.5 tail vein injection to evaluate the renal targeting ability of NPs. Mice were euthanized at different times (3, 6, 12, 24, 48 h) after Sham or I/R, and their main organs were harvested for optical imaging technology. Results showed NPs had renal targeting ability. In the Sham group, NPs could pass through the glomerular vascular endothelium via particle size and accumulated in kidneys, but NPs were blocked in the glomerulus by the intact podocyte barrier and metabolized after 12 h (Fig. 4B, C). In the I/R group, MMP2 was expressed and the GFB was disrupted, enabling NPs to target the kidney and stably accumulate. Fluorescence could be maintained for up to 48 h, indicating that NPs released drugs targeting renal injury cells after being lysed by ROS and MMP2 (Fig. 4B, D). We also linked FITC to the skeleton structure of NPs via NH_2, and after the Sham or I/R 12 h, organs were harvested for fluorescence scanning. For the heart, liver, spleen, and lungs, the particle size of the vascular endothelium is only about 10 nm, through which NPs cannot pass [21]. Therefore, the fluorescence results only indicated that some NPs adhered to the inner of the blood vessels and did not extravasate to tissues. The blood vessels in the liver expanded due to the higher portal pressure, which also explained the reason for the higher fluorescence intensity in the liver. However, for the kidneys, the larger pore size of the vascular fenestrations allowed the passage of NPs. Therefore, in the Sham group, the fluorescence analysis showed that in addition to the vascular morphology, NPs also accumulated in the glomeruli, which were blocked by the podocyte barrier. In the I/R group, with the destruction of GFB, NPs could pass through GFB and target renal injury cells (Fig. 4E).

NPs reduce ROS and alleviate AKI in vivo

To investigate the effect of NPs on I/R-AKI, renal function was measured after 12 h of I/R. NPs could significantly reduce the elevation of Scr (50.66 ± 3.75 in I/R + NPs vs. 70.85 ± 3.84 μmol/L in I/R + Saline) and BUN (25.18 ± 1.59 in I/R + NPs vs. 35.03 ± 2.86 mg/dl in I/R + Saline) after I/R (Fig. 5A, B). Additionally, NPs decreased the mRNA levels of AKI biomarkers (38% decrease in NGAL and 34% decrease in KIM-1) following I/R (Fig. 5C, D). HE staining showed that NPs could reduce renal pathological damage, and reduce the tubular injury scores by 35% (Fig. 5E, F). TUNEL staining was used to detect the apoptosis of kidney cells, and NPs could reduce the apoptosis (27.52 ± 2.54‰ in I/R + NPs vs. 44.63 ± 4.68‰ in I/R + Saline) (Fig. 5G, H). Oxidative stress is an important characteristic of renal I/R. We homogenized kidney tissues and measured the levels of SOD and MDA. NPs could significantly alleviate the loss of renal antioxidant activity (31% decrease in MDA and 1.30-fold increase in SOD) (Fig. 5I, J). DHE staining

(See figure on next page.)

Fig. 5 NPs reduce ROS and alleviate AKI in vivo. **A**. Serum creatinine levels of Sham or I/R groups treated with Saline or NPs. **B**. BUN levels of Sham or I/R groups treated with Saline or NPs. **C**. NGAL mRNA expression of Sham or I/R groups treated with Saline or NPs. **D**. KIM-1 mRNA expression of Sham or I/R groups treated with Saline or NPs. **E**. Representative histological HE staining in kidneys of Sham or I/R groups treated with Saline or NPs, scale bar = 50 μm. **F**. Tubular injury scores of HE staining. **G**. Representative TUNEL staining in kidneys of Sham or I/R groups treated with Saline or NPs, scale bar = 20 μm. **H**. TUNEL-positive cells rate of TUNEL staining. **I.** MDA levels of Sham or I/R groups treated with Saline or NPs. **J**. SOD levels of Sham or I/R groups treated with Saline or NPs. **K**. Representative DHE staining in kidneys of Sham or I/R groups treated with Saline or NPs, scale bar = 50 μm. **L**. Relative fold of DHE staining. Results are presented as means ± SEM, n = 6. P values from Student's t test. * indicates $P < 0.05$; ** indicates $P < 0.01$; *** indicates $P < 0.001$

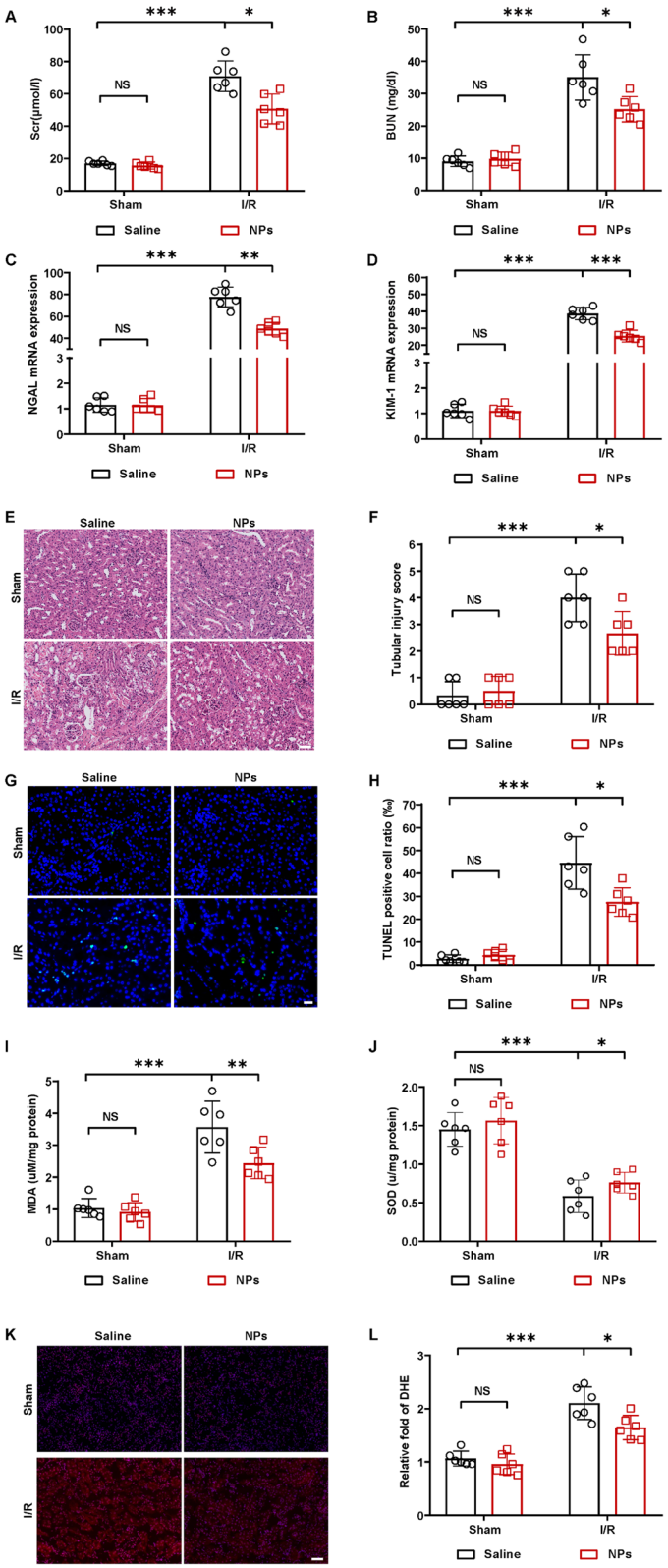

Fig. 5 (See legend on previous page.)

also demonstrated that NPs could reduce ROS by 22% (Fig. 5K, L).

NPs reduce AKI by inhibiting ferroptosis in vivo

After demonstrating the therapeutic effect of NPs on AKI, we analyzed its therapeutic mechanism through RNA sequencing. Between the I/R groups, NPs inhibited the expression of Lcn2 (NGAL) and Havcr1 (KIM-1), and to some extent reduced the expression of MMP2. Since the NPs with diselenide shell wrapped VitE, the NPs inhibited the expression of ferroptosis related genes, including genes related to lipid peroxidation, iron ion metabolism, etc. (Fig. 6A). KEGG results showed changes in pathways closely related to I/R, such as inflammation, lipid metabolism, oxidative stress, and apoptosis, indicating that NPs play a significant role in I/R (Fig. 6B). We also conducted gene ontology enrichment, in Biological Processes, NPs altered the metabolism of reactive oxygen species, fatty acids, and metal ions, especially iron ions, in addition to vitamin transport and metabolic process. In Cellular Component, NPs participated in extracellular matrix, plasma membrane, podosome, etc., indicating that NPs alleviates the damage to the renal filtration barrier structure caused by I/R. Additionally, NPs could regulate peroxisomes and ion channels. In Molecular Function, VitE functioned as an antioxidant and inhibitor of ferroptosis, and its mechanism was to react with peroxide free radicals, thereby blocking the lipid peroxidation chain reaction. We detected changes in the activity of oxidoreductases acting on CH-CH and CH-OH. In addition, NPs also regulated a series of ferroptosis related molecular function, including iron ion binding, CoA-ligase activity, fatty acids, and glutathione (Fig. 6C). To clarify the regulatory function of NPs, we conducted GSEA analysis. The results showed that NPs significantly upregulated the VITAMIN binding of kidney, indicating the renal targeting ability of NPs. The results also showed that NPs significantly increased the activity acting on the CH-CH and CH-OH group of donors, corresponding to VitE inhibiting ferroptosis by blocking the lipid peroxidation chain reaction via LO• and LOO• (Fig. 6D). Next, we detected the expression of ACSL4, ALOX5, and 4hydroxynonenal (4HNE), the end product of ferroptosis, by western blotting. The results showed that NPs could inhibit the expression of ACSL4 and ALOX5, reducing the production of 4HNE (Fig. 6E, F). Additionally, we performed 4HNE immunohistochemistry staining, and NPs can reduce ferroptosis by 28% (Fig. 6G, H).

NPs reduce ROS and inhibit ferroptosis in vitro

We analyzed oxidative stress in HK-2 cells exposed to H/R by DHE staining. After H/R, ROS in HK-2 cells was increased. However, NPs inhibited H/R induced ROS in HK-2 cells by 29% (Fig. 7A, B). We quantified ROS by flow cytometry and the results showed that NPs reduced ROS by 33% (Fig. 7C, D). Additionally, we detected changes in ferroptosis related proteins. NPs could inhibit the expression of ACSL4 and ALOX5, reducing the production of 4HNE (Fig. 7E, F). 4HNE fluorescence intensity was reduced by 25%, demonstrating that NPs can reduce ferroptosis in vitro (Fig. 7G, H).

NPs attenuates the transition of AKI to CKD

AKI is an independent risk factor for CKD and end-stage renal disease, and approximately 70% of AKI patients are at risk of developing CKD and renal failure [22]. Incomplete repair of acute tubular injury can lead to irreversible fibrosis in the kidneys. To analyze the effect of NPs on the progression of AKI to CKD, 30-min bilateral I/R-induced AKI-to-CKD models were constructed. First, in the Sham group, 14 days after injecting NPs, the histopathological analysis and blood tests also showed no significant abnormalities, ensuring the long-term biosafety of NPs (Fig. S 2 C&D). Masson and Picrosirius Red were used to detect the deposition of collagen fibers in the tissue, and NPs could reduce the fibrotic area by 27.9% (Fig. 8A, B). During this process, we measured Scr at different times, and NPs treatment could promote the early recovery of renal function and reduce the irreversible loss of renal function in the late stage (Fig. 6C). Immunohistochemistry detected that the Collagen 1 and fibrotic markers α-smooth muscle actin (α-SMA) were expressed in the I/R groups, while the NPs reduced the positive area, indicating that NPs effectively prevented renal fibrosis (Fig. 8D–G). In addition, we also semi-quantified by WB that NPs could reduce Collagen 1 by 25.4% and α-SMA by 32.3% (Fig. 8H, I).

(See figure on next page.)

Fig. 6 NPs reduce ROS and alleviate AKI in vivo. **A**. Heat map analysis for RNA-sequencing of I/R group treated with Saline or NPs. **B**. KEGG pathway classification analysis of I/R group treated with Saline or NPs. **C**. GO enrichment of I/R group treated with Saline or NPs. **D**. GSEA analysis of I/R group treated with Saline or NPs. **E**. Representative western blotting of ferroptosis-related protein in Sham or I/R groups treated with Saline or NPs. **F**. Protein levels analysis of western blotting. **G**. Representative immunohistochemical staining images of 4HNE in Sham or I/R groups treated with Saline or NPs, scale bar = 50 μm. **H**. 4HNE Positive area percentage of immunohistochemical staining. Results are presented as means ± SEM, n = 6. P values from Student's t test. * indicates $P < 0.05$; ** indicates $P < 0.01$; *** indicates $P < 0.001$

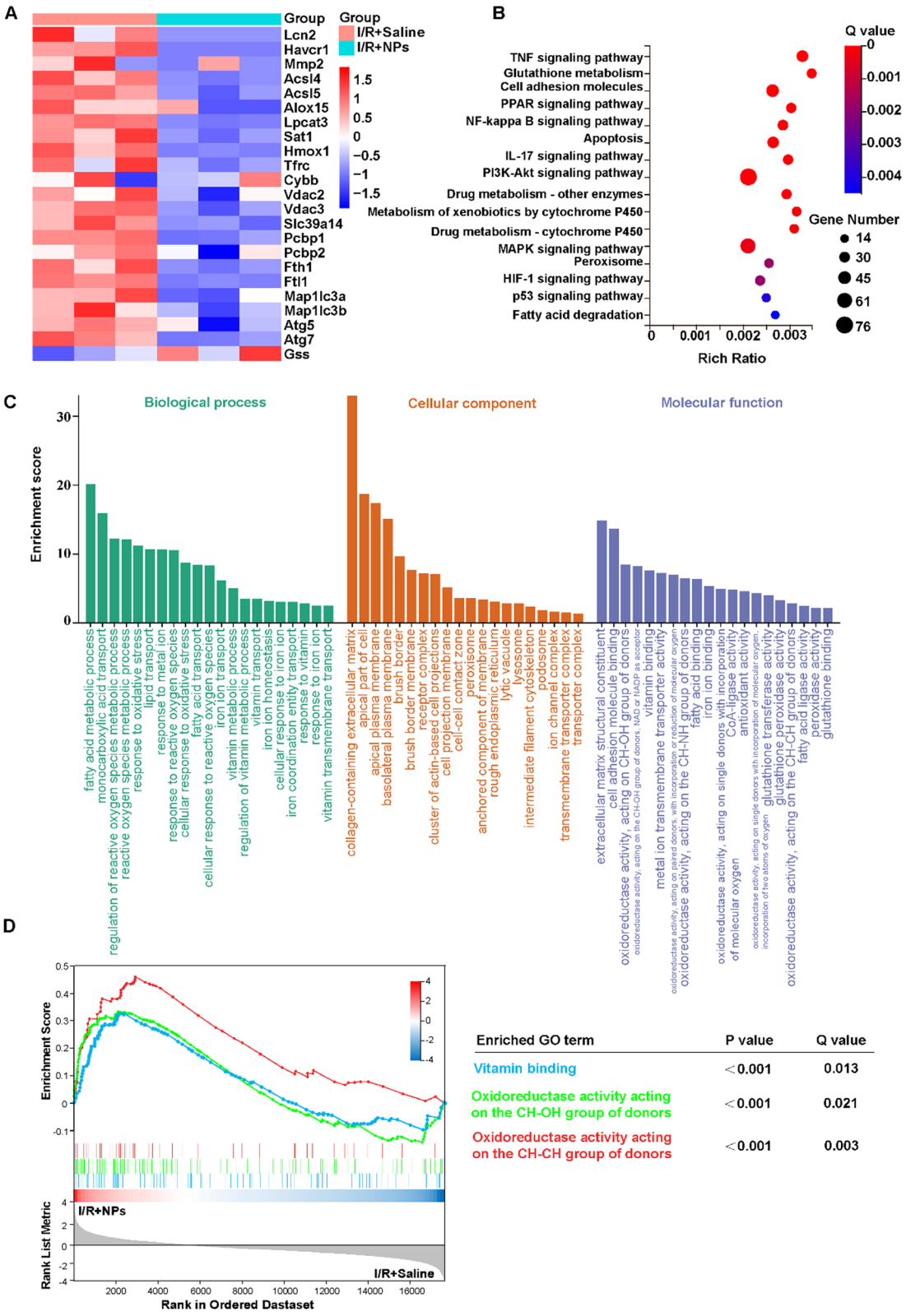

Fig. 6 (See legend on previous page.)

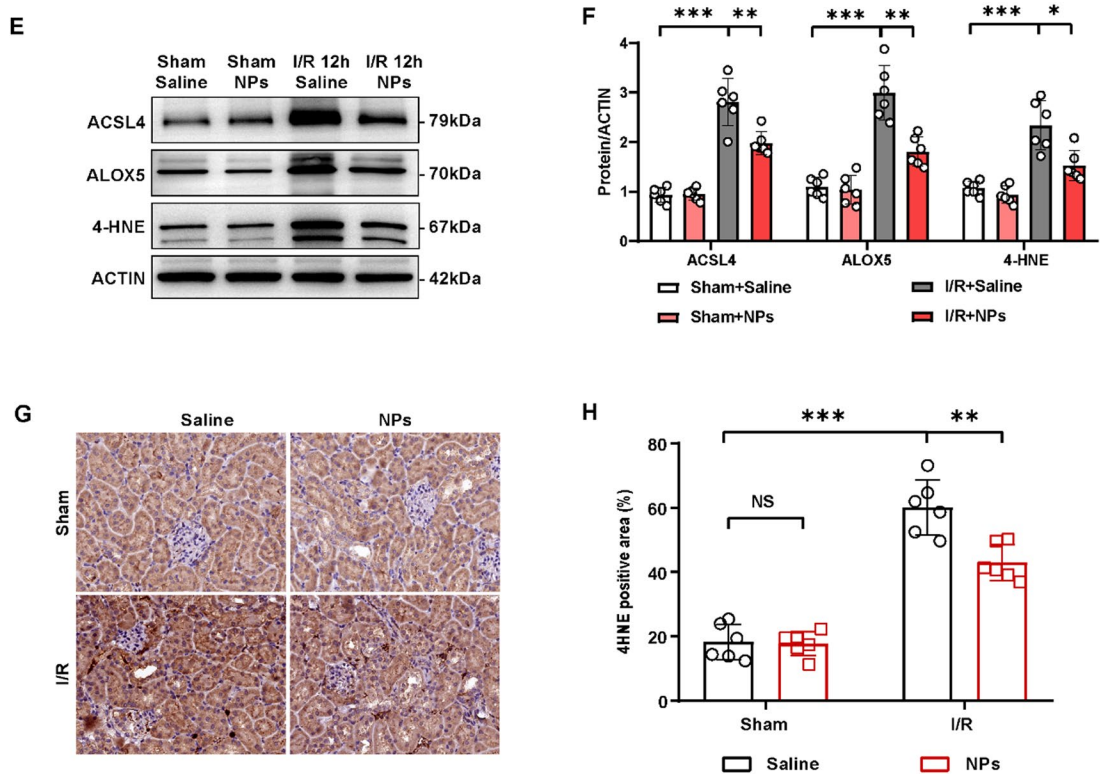

Fig. 6 continued

Discussion

Our strategy for synthesizing the NPs is through the self-assembly of amphiphilic polymers. In aqueous environments (saline or PBS), these amphiphilic polymers, Gel-SH and DSPE-Se-Se-PEG_{2k}-NH_2, undergo self-assembly as the differential solubility of their different part of segments. These hydrophobic segments have low solubility in water and thus aggregate through hydrophobic interactions to form a core, which is surrounded by a hydrophilic shell to form a spherical micelle structure This configuration facilitates the effective encapsulation of hydrophobic VitE within the micelle core. The particle size results indicated that the particle size was 69.92 nm. Furthermore, the morphology of the NPs can be determined by adjusting the molecular weight ratio between the hydrophilic and hydrophobic segments. In specific, with the large molecular weight of the hydrophobic segment, the formed micelles are cylindrical and have a larger particle size. Such ability to fine-tune the structure highlights the versatility of the self-assembling amphiphilic polymers, making it possible to synthesize nanoparticles with various morphologies and sizes, thereby greatly broadening the application potential in medicine delivery. These formed NPs with a hydrodynamic size less than 100 nm, exhibiting dual-responsiveness to MMP2 and ROS, effectively target and deliver VitE to renal injured cells, demonstrating a significant role in suppressing ROS and ferroptosis. Following tail vein injection, the NPs efficiently accumulate in the kidneys and traverse the GFB damaged by I/R. Both in vitro and in vivo experiments have confirmed the biocompatibility and targeting ability towards renal injured cells of NPs. In vivo results indicate that the NPs can inhibit ROS and renal function damage

(See figure on next page.)

Fig. 7 NPs reduce ROS and inhibit ferroptosis in vitro. **A**. Representative DHE staining in HK-2 of H/R 0 h or 12 h groups treated with PBS or NPs, scale bar = 20 μm. **B**. Mean fluorescence intensity of DHE staining. **C**. Representative histogram showing ROS in HK-2 of H/R 0 h or 12 h groups treated with PBS or NPs. **D**. Relative fold of ROS. **E**. Representative western blotting of ferroptosis-related protein in HK-2 of H/R 0 h or 12 h groups treated with PBS or NPs. **F**. Protein levels analysis of western blotting. **G**. Representative immunofluorescence staining images of 4HNE in HK-2 of H/R 0 h or 12 h groups treated with PBS or NPs, scale bar = 20 μm. **H**. Mean fluorescence intensity of immunofluorescence staining images for 4HNE. Results are presented as means ± SEM, n = 6. P values from Student's t test. * indicates $P < 0.05$; ** indicates $P < 0.01$; *** indicates $P < 0.001$

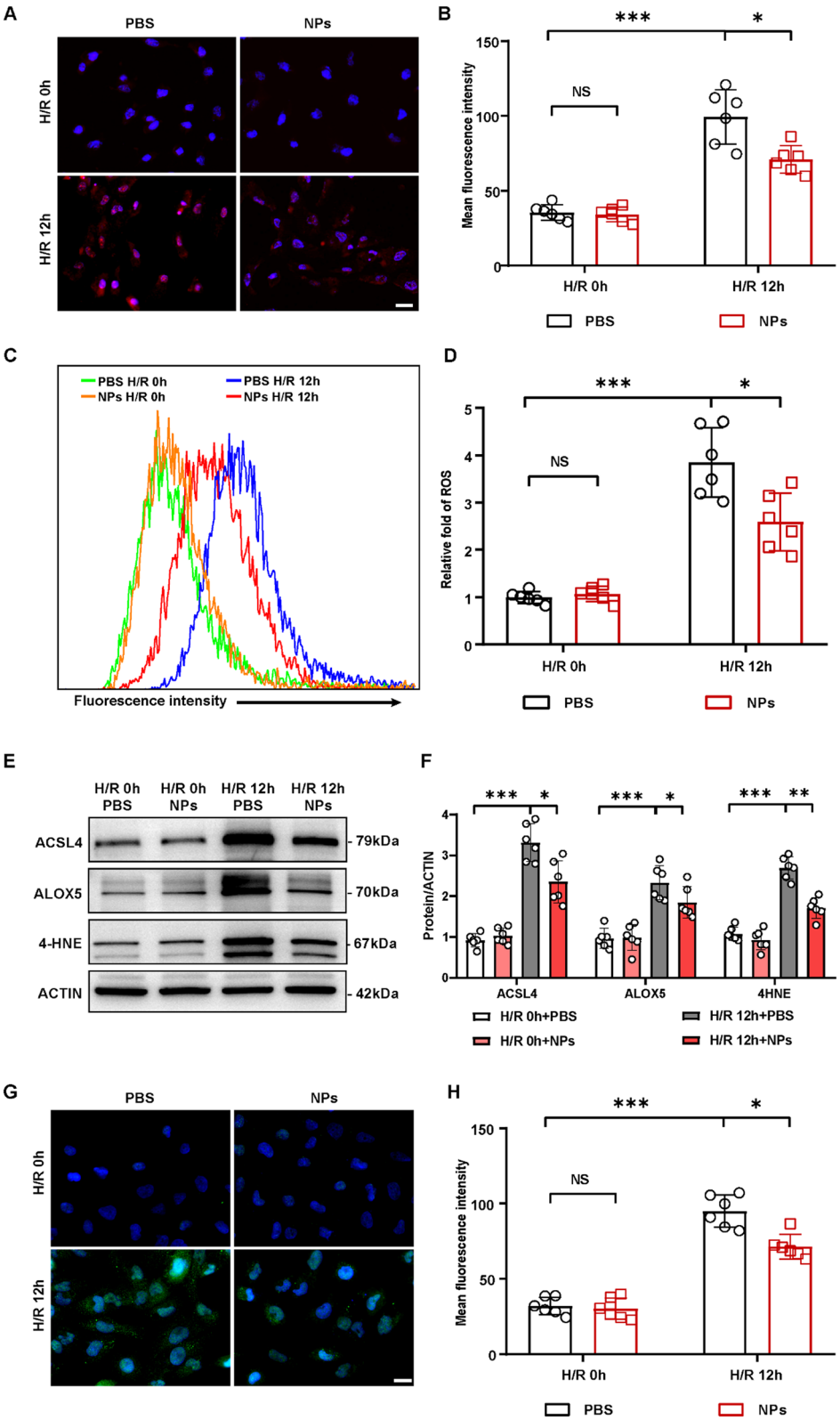

Fig. 7 (See legend on previous page.)

following I/R. RNA sequencing results suggest that the NPs exert their therapeutic effects by suppressing ferroptosis. Finally, we have also demonstrated that the NPs can reduce ROS and inhibit ferroptosis in vitro.

The GFB consists of glomerular endothelial cells, glomerular basement membrane (GBM), and podocytes [23]. The pore size of glomerular endothelial cells typically has a relatively wide width of 70 to 130 nm, and NPs below 130 nm can be selectively filtered by the kidneys [17]. The NPs have a hydrodynamic size of 69.92 nm and can pass through the pore of glomerular endothelial cell. The GBM has a pore size of 2–8 nm, and podocytes have a monolayer of cells with a pore size of 4–11 nm [24]. Normally, NPs of 100 nm can pass through endothelial cell pores but are blocked by the GBM and the intact podocyte barrier, which is consistent with the podocyte fluorescence and organ imaging results of Sham group in our study. However, after I/R, the enzyme MMP2 for matrix remodeling is expressed on the peritubular capillary endothelial cells, causing GBM degradation, podocyte damage, and increased glomerular permeability, enabling large substances to pass through [25, 26]. Related studies have shown that GFB structure is disrupted by I/R, and its permeability undergoes significant changes, allowing 100 nm NPs to be delivered to renal tubules [18]. The fluorescence of podocytes showed that the podocyte barrier of the I/R group was disrupted, MMP2 was expressed, and NPs began to accumulate in the kidney at 3 h. Besides, it still shows fluorescence until 48 h, indicating that NPs has been cleaved and VitE was released.

MMP2 is one of the zinc-dependent proteases, and responsible for extracellular matrix breakdown and bioactive protein degradation, which is involved in I/R [27]. MMP2 can increase 10 min after I/R and maintain a sustained increase [28]. In this study, substrate Gel of MMP2 was used as the shell material. After NPs delivery to the kidneys, the Gel shell can achieve the effect of targeting and releasing drugs to renal injury cells. Moreover, it can competitively neutralize MMP2, thereby inhibiting its further damage to kidney. Due to the important binding of selenium as a glutathione peroxidase and thioredoxin reductase with selenium dependent enzymes, selenium effectively neutralizes free radicals and maintains intracellular redox balance [29]. Multiple selenium-based NPs have been proven to inhibit the occurrence and development of AKI [30–32]. We employed diselenide to react with ROS, enabling targeted drug delivery, neutralizing ROS, and replenishing selenium. The most crucial factor for guiding nanoparticles to kidney and avoiding phagocytosis mediated by the mononuclear phagocyte system is their relatively non-opsonic surface. Long PEG chains (> 2000 Da) are most effective in reducing regulatory effects [1, 33, 34]. In our study, we prepared PEG_{2k} on NPs. Although NPs temporarily accumulate in the liver due to inferior vena cava pressure after tail vein injection, NPs rapidly decreases and demonstrate renal targeting ability. Besides, the low fluorescence intensity in the spleen, which also possessed mononuclear phagocyte system like the liver, similarly demonstrated the effectiveness of PEGylated in resisting phagocytosis. The increase in fluorescence intensity in the liver was due to the temporary accumulation of drugs caused by the opening of the portal vein.

Ferroptosis is a chain reaction initiated by iron-dependent interactions between LOO• and PUFA, resulting in the formation of L•, which subsequently regenerates LOO•. The reaction rate between VitE and LOO• is 1000 times faster compared to that between LOO• and PUFA. Consequently, the targeted delivery of VitE effectively inhibits the formation of L•, preventing chain reactions and thus inhibiting ferroptosis [35]. Related studies have shown that the concentration of VitE in human plasma is only about 15 μM [36]. Animal experiments have shown that VitE supplementation can alleviate AKI caused by cisplatin and I/R [37, 38]. A prospective double-blind study on humans showed that VitE can reduce contrast-induced AKI [39]. Studies in human also demonstrated that VitE can reduce the renal toxicity of drugs [40, 41]. However, high-dose supplementation of VitE throughout the body may lead to bleeding and increased mortality [14, 42]. Therefore, targeted renal supplementation with VitE is an effective strategy for treating AKI.

CKD imposes a huge burden on global public health as current therapies are generally ineffective. Early detection and effective treatment are crucial for the future

(See figure on next page.)

Fig. 8 NPs attenuates the transition of AKI to CKD. **A**. Representative histological Masson and Picrosirius Red staining in kidneys of Sham or I/R 14d groups treated with Saline or NPs, scale bar = 50 μm. **B**. Mean Fibrotic area of staining. **C**. Serum creatinine levels at different times of Sham or I/R groups treated with Saline or NPs. **D**. Representative immunohistochemical staining images of Collagen 1 in Sham or I/R 14d groups treated with Saline or NPs, scale bar = 20 μm. **E**. Collagen 1 Positive area percentage of immunohistochemical staining. **F**. Representative immunohistochemical staining images of α-SMA in Sham or I/R 14d groups treated with Saline or NPs, scale bar = 20 μm. **G**. α-SMA Positive area percentage of immunohistochemical staining. **H**. Representative western blotting of fibrotic-related protein in Sham or I/R 14d groups treated with Saline or NPs. **I**. Protein levels analysis of western blotting. Results are presented as means ± SEM, n = 6. P values from Student's t test. * indicates $P < 0.05$; ** indicates $P < 0.01$; *** indicates $P < 0.001$

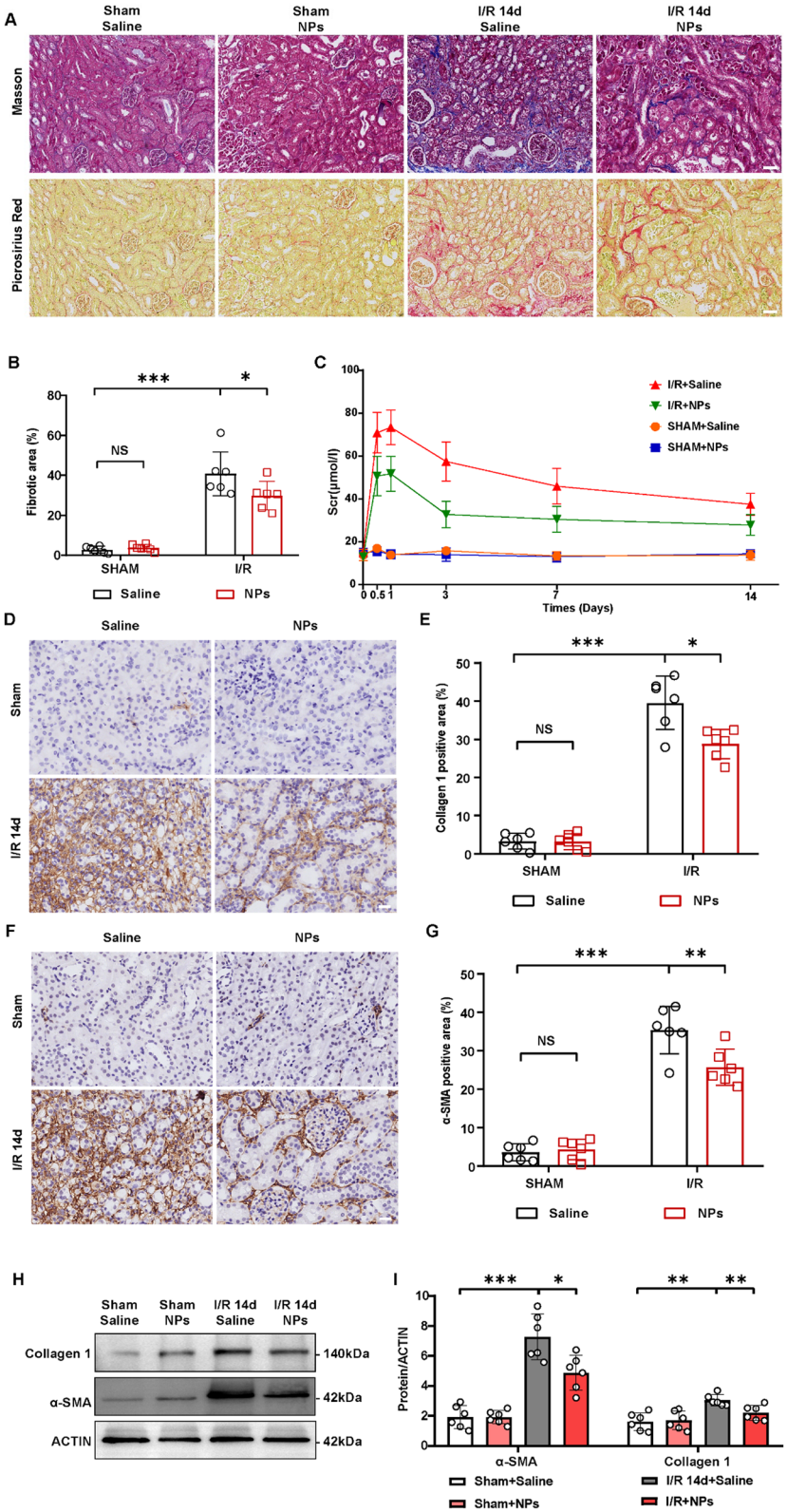

Fig. 8 (See legend on previous page.)

prevention and progression of CKD [43]. Increasing evidence suggests that kidney-targeted NPs are one of the effective methods for the prevention and treatment of CKD, which can improve the bioavailability of drugs, reduce toxicity, and reduce the filtration pressure of the kidneys [22, 44]. In our study, we investigated the effect of NPs in the AKI-CKD model induced by I/R. We found that VitE-loaded NPs could reduce the accumulation of collagen fibers at 14 days, promote the recovery of AKI, and reduce the irreversible loss of renal function, thus retarding the transition of AKI to CKD.

Conclusion

In conclusion, we synthesized the NPs that target renal injury cells for VitE delivery through dual-response to MMP2 and ROS. The NPs have good biocompatibility and targeting ability to renal injury cells. The NPs could reduce ROS, reduce ferroptosis, alleviate I/R-AKI and inhibit the transition from AKI to CKD. The NPs may provide a novel therapy for I/R-induced kidney disease.

Supplementary Information

The online version contains supplementary material available at https://doi.org/10.1186/s12951-024-02894-7.

Supplementary material 1.

Acknowledgements
We appreciate the technical support provided by Wang Taibing.

Author contributions
J.Z and X.R designed this study; J.Z, X.R and Z.N were responsible for the experiments, Z.N, Y.Y, Y.Z and H.C were responsible for the data collection; J.Z, X.R, Z.N, G.M and H.Y were responsible for data analysis; J.Z, X.R, Z.N and L.S conducted the manuscript writing; Z.P and L.S critically revised the manuscript, Z.P and M.-C. Tang approved the final version to be published; all authors agreed to be accountable for all aspects of the work in ensuring that questions related to the accuracy or integrity of any part of the work are appropriately investigated and resolved.

Funding
This work was supported by the National Natural Science Foundation (No. 82102298 to Dr Su, and No. 81772046 and No. 81971816 to Dr Peng).

Availability of data and materials
All mRNA-Seq data has been made publicly available via PubMed with BioProject ID: PRJNA1152106. SRA records are accessible with the following link: https://www.ncbi.nlm.nih.gov/sra/PRJNA1152106.

Declarations

Ethics approval and consent to participate
All animal experiments were approved by The Animal Care and Use Committee of Zhongnan Hospital of Wuhan University and the approved number was WP20230685.

Competing interests
The authors declare no competing interests.

Author details
[1]Department of Critical Care Medicine, Zhongnan Hospital of Wuhan University, Wuhan 430000, Hubei, China. [2]Clinical Research Center of Hubei Critical Care Medicine, Wuhan, China. [3]Dyson School of Design Engineering, Imperial College London, London SW7 2BX, UK. [4]Institute of Materials Research, Tsinghua Shenzhen International Graduate School, Tsinghua University, Shenzhen 518000, China. [5]Department of Cardiology, David Geffen School of Medicine, University of California, Los Angeles, CA, USA. [6]Center of Critical Care Nephrology, Department of Critical Care Medicine, University of Pittsburgh Medical Center, Pittsburgh, USA.

Received: 18 July 2024 Accepted: 2 October 2024
Published online: 15 October 2024

References

1. Huang Y, Ning X, Ahrari S, Cai Q, Rajora N, Saxena R, Yu M, Zheng J. Physiological principles underlying the kidney targeting of renal nanomedicines. Nat Rev Nephrol. 2024. https://doi.org/10.1038/s41581-024-00819-z.
2. Zhang J, Long M, Sun Z, Yang C, Jiang X, He L, Su L, Peng Z. Association between Thymosin beta-4, acute kidney injury, and mortality in patients with sepsis: An observational cohort study. Int Immunopharmacol. 2021;101: 108167.
3. Ehmann MR, Klein EY, Zhao X, Mitchell J, Menez S, Smith A, Levin S, Hinson JS. Epidemiology and clinical outcomes of community-acquired acute kidney injury in the emergency department: a multisite retrospective cohort study. Am J Kidney Dis. 2023. https://doi.org/10.1053/j.ajkd.2023.10.009.
4. Mehta RL, Cerda J, Burdmann EA, Tonelli M, Garcia-Garcia G, Jha V, Susantitaphong P, Rocco M, Vanholder R, Sever MS, et al. International society of nephrology's 0by25 initiative for acute kidney injury (zero preventable deaths by 2025): a human rights case for nephrology. Lancet. 2015;385(9987):2616–43.
5. Pereira BJ, Barreto S, Gentil T, Assis LS, Soeiro EM, Castro I, Laranja SM. Risk factors for the progression of chronic kidney disease after acute kidney injury. J Bras Nefrol. 2017;39(3):239–45.
6. Dixon SJ, Lemberg KM, Lamprecht MR, Skouta R, Zaitsev EM, Gleason CE, Patel DN, Bauer AJ, Cantley AM, Yang WS, et al. Ferroptosis: an iron-dependent form of nonapoptotic cell death. Cell. 2012;149(5):1060–72.
7. Hadian K, Stockwell BR. SnapShot: ferroptosis. Cell. 2020;181(5):1188–1188.
8. Bhargava P, Schnellmann RG. Mitochondrial energetics in the kidney. Nat Rev Nephrol. 2017;13(10):629–46.
9. Xu Z, Zhu Y, Xie M, Liu K, Cai L, Wang H, Li D, Chen H, Gao L. Mackinawite nanozymes as reactive oxygen species scavengers for acute kidney injury alleviation. J Nanobiotechnology. 2023;21(1):281.
10. Feng Q, Yang Y, Ren K, Qiao Y, Sun Z, Pan S, Liu F, Liu Y, Huo J, Liu D, et al. Broadening horizons: the multifaceted functions of ferroptosis in kidney diseases. Int J Biol Sci. 2023;19(12):3726–43.
11. Su L, Zhang J, Wang J, Wang X, Cao E, Yang C, Sun Q, Sivakumar R, Peng Z. Pannexin 1 targets mitophagy to mediate renal ischemia/reperfusion injury. Commun Biol. 2023;6(1):889.
12. Saito Y. Lipid peroxidation products as a mediator of toxicity and adaptive response - The regulatory role of selenoprotein and vitamin E. Arch Biochem Biophys. 2021;703: 108840.
13. Hu Q, Zhang Y, Lou H, Ou Z, Liu J, Duan W, Wang H, Ge Y, Min J, Wang F, et al. GPX4 and vitamin E cooperatively protect hematopoietic stem and progenitor cells from lipid peroxidation and ferroptosis. Cell Death Dis. 2021;12(7):706.
14. Miller ER 3rd, Pastor-Barriuso R, Dalal D, Riemersma RA, Appel LJ, Guallar E. Meta-analysis: high-dosage vitamin E supplementation may increase all-cause mortality. Ann Intern Med. 2005;142(1):37–46.
15. Vallorz EL, Janda J, Mansour HM, Schnellmann RG. Kidney targeting of formoterol containing polymeric nanoparticles improves recovery from ischemia reperfusion-induced acute kidney injury in mice. Kidney Int. 2022;102(5):1073–89.
16. Li J, Duan Q, Wei X, Wu J, Yang Q. Kidney-targeted nanoparticles loaded with the natural antioxidant rosmarinic acid for acute kidney injury treatment. Small. 2022;18(48): e2204388.

17. Liu CP, Hu Y, Lin JC, Fu HL, Lim LY, Yuan ZX. Targeting strategies for drug delivery to the kidney: from renal glomeruli to tubules. Med Res Rev. 2019;39(2):561–78.
18. Yu H, Lin T, Chen W, Cao W, Zhang C, Wang T, Ding M, Zhao S, Wei H, Guo H, et al. Size and temporal-dependent efficacy of oltipraz-loaded PLGA nanoparticles for treatment of acute kidney injury and fibrosis. Biomaterials. 2019;219: 119368.
19. Zhou K, Zhu Y, Chen X, Li L, Xu W. Redox- and MMP-2-sensitive drug delivery nanoparticles based on gelatin and albumin for tumor targeted delivery of paclitaxel. Mater Sci Eng C Mater Biol Appl. 2020;114: 111006.
20. Kilkenny C, Browne WJ, Cuthill IC, Emerson M, Altman DG. Improving bioscience research reporting: the ARRIVE guidelines for reporting animal research. PLoS Biol. 2010;8(6): e1000412.
21. Tee JK, Yip LX, Tan ES, Santitewagun S, Prasath A, Ke PC, Ho HK, Leong DT. Nanoparticles' interactions with vasculature in diseases. Chem Soc Rev. 2019;48(21):5381–407.
22. Kong Y, Chen X, Liu F, Tang J, Zhang Y, Zhang X, Zhang L, Zhang T, Wang Y, Su M, et al. Ultrasmall polyphenol-NAD(+) nanoparticle-mediated renal delivery for mitochondrial repair and anti-inflammatory treatment of akito-ckd progression. Adv Mater. 2024;36(30): e2310731.
23. Wang D, Sant S, Ferrell N. A biomimetic In vitro model of the kidney filtration barrier using tissue-derived glomerular basement membrane. Adv Healthc Mater. 2021;10(16): e2002275.
24. Jiang D, Rosenkrans ZT, Ni D, Lin J, Huang P, Cai W. Nanomedicines for renal management: from imaging to treatment. Acc Chem Res. 2020;53(9):1869–80.
25. Kunugi S, Shimizu A, Kuwahara N, Du X, Takahashi M, Terasaki Y, Fujita E, Mii A, Nagasaka S, Akimoto T, et al. Inhibition of matrix metalloproteinases reduces ischemia-reperfusion acute kidney injury. Lab Invest. 2011;91(2):170–80.
26. Rippe C, Rippe A, Larsson A, Asgeirsson D, Rippe B. Nature of glomerular capillary permeability changes following acute renal ischemia-reperfusion injury in rats. Am J Physiol Renal Physiol. 2006;291(6):F1362-1368.
27. Ceron CS, Baligand C, Joshi S, Wanga S, Cowley PM, Walker JP, Song SH, Mahimkar R, Baker AJ, Raffai RL, et al. An intracellular matrix metalloproteinase-2 isoform induces tubular regulated necrosis: implications for acute kidney injury. Am J Physiol Renal Physiol. 2017;312(6):F1166–83.
28. McNair ED, Bezaire J, Moser M, Mondal P, Conacher J, Franczak A, Sawicki G, Reid D, Khani-Hanjani A. The Association of matrix metalloproteinases with acute kidney injury following CPB-supported cardiac surgery. Can J Kidney Health Dis. 2021;8:20543581211019640.
29. Pei J, Pan X, Wei G, Hua Y. Research progress of glutathione peroxidase family (GPX) in redoxidation. Front Pharmacol. 2023;14:1147414.
30. Bao B, Liu H, Han Y, Xu L, Xing W, Li Z. Simultaneous elimination of reactive oxygen species and activation of Nrf2 by ultrasmall nanoparticles to relieve acute kidney injury. ACS Appl Mater Interfaces. 2023;15(13):16460–70.
31. Wang S, Chen Y, Han S, Liu Y, Gao J, Huang Y, Sun W, Wang J, Wang C, Zhao J. Selenium nanoparticles alleviate ischemia reperfusion injury-induced acute kidney injury by modulating GPx-1/NLRP3/Caspase-1 pathway. Theranostics. 2022;12(8):3882–95.
32. Li X, Wang Q, Deng G, Liu Y, Wei B, Liu X, Bao W, Wang Q, Wu S. Porous Se@SiO2 nanospheres attenuate cisplatin-induced acute kidney injury via activation of Sirt1. Toxicol Appl Pharmacol. 2019;380: 114704.
33. Williams RM, Shah J, Ng BD, Minton DR, Gudas LJ, Park CY, Heller DA. Mesoscale nanoparticles selectively target the renal proximal tubule epithelium. Nano Lett. 2015;15(4):2358–64.
34. Shang S, Li X, Wang H, Zhou Y, Pang K, Li P, Liu X, Zhang M, Li W, Li Q, et al. Targeted therapy of kidney disease with nanoparticle drug delivery materials. Bioact Mater. 2024;37:206–21.
35. Traber MG, Head B. Vitamin E: How much is enough, too much and why! Free Radic Biol Med. 2021;177:212–25.
36. Traber MG. Human Vitamin E deficiency, and what is and is not Vitamin E? Free Radic Biol Med. 2024;213:285–92.
37. Abo-Elmaaty AMA, Behairy A, El-Naseery NI, Abdel-Daim MM. The protective efficacy of vitamin E and cod liver oil against cisplatin-induced acute kidney injury in rats. Environ Sci Pollut Res Int. 2020;27(35):44412–26.
38. Koga H, Hagiwara S, Mei H, Hiraoka N, Kusaka J, Goto K, Kashima K, Noguchi T. The vitamin E derivative, ESeroS-GS, attenuates renal ischemia-reperfusion injury in rats. J Surg Res. 2012;176(1):220–5.
39. Tasanarong A, Vohakiat A, Hutayanon P, Piyayotai D. New strategy of alpha- and gamma-tocopherol to prevent contrast-induced acute kidney injury in chronic kidney disease patients undergoing elective coronary procedures. Nephrol Dial Transplant. 2013;28(2):337–44.
40. Samsami M, Shabani M, Hajiesmaeili M, Tavakoli-Ardakani M, Ardehali SH, Fatemi A, Barati S, Moradi O, Sahraei Z. The effects of vitamin E on colistin-induced nephrotoxicity in treatment of drug-resistant gram-negative bacterial infections: A randomized clinical trial. J Infect Chemother. 2021;27(8):1181–5.
41. Soltani R, Khorvash F, Meidani M, Badri S, Alaei S, Taheri S. Vitamin E in the prevention of vancomycin-induced nephrotoxicity. Res Pharm Sci. 2020;15(2):137–43.
42. Lee IM, Cook NR, Gaziano JM, Gordon D, Ridker PM, Manson JE, Hennekens CH, Buring JE. Vitamin E in the primary prevention of cardiovascular disease and cancer: the Women's Health Study: a randomized controlled trial. JAMA. 2005;294(1):56–65.
43. Ma Y, Cai F, Li Y, Chen J, Han F, Lin W. A review of the application of nanoparticles in the diagnosis and treatment of chronic kidney disease. Bioact Mater. 2020;5(3):732–43.
44. Qin S, Liu C, Chen Y, Yao M, Liao S, Xin W, Gong S, Guan X, Li Y, Xiong J, et al. Cobaltosic oxide-polyethylene glycol-triphenylphosphine nanoparticles ameliorate the acute-to-chronic kidney disease transition by inducing BNIP3-mediated mitophagy. Kidney Int. 2023;103(5):903–16.

Publisher's Note